Journal of Space Safety Engineering xxx (xxxx) xxx

Contents lists available at ScienceDirect

Journal of Space Safety Engineering

journal homepage: www.elsevier.com/locate/jsse

Launch & Reentry Systems

Full-scale simulation and analysis of formation flight during in-air-capturing of a winged reusable launch vehicle

Sunayna Singh[a,*], Sven Stappert[a], Leonid Bussler[a], Martin Sippel[a], Yakut Cansev Kucukosman[b], Sophia Buckingham[b]

[a] DLR Institut für Raumfahrtsysteme, Linzer Straße 1, 28359, Bremen, Germany
[b] von Karman Institute for Fluid Dynamics VKI, 72 Chaussée de Waterloo, Rhode-St-Genèse B-1640, Belgium

ARTICLE INFO

Article history:
Received 17 February 2022
Received in revised form 2 September 2022
Accepted 26 September 2022
Available online xxx

Keywords:
FALCon
In-air-capturing
Reusable launch systems
Vertical take-off horizontal landing
Formation flight
Sustainable space

ABSTRACT

In the past two decades, the renewed interest in sustainable space transportation has driven the development of many innovative reusable launch technologies. One such concept called 'In-Air-Capturing (IAC)' involves winged rocket stages captured mid-air and towed back to the launch site using an aircraft. The approach, patented by German Aerospace Centre (DLR), shows potential for substantial mass and cost reduction by eliminating the need for additional propulsion during the descent. A critical aspect of IAC requires the two involved vehicles to be in a parallel formation with similar velocities and altitudes separated by a safe distance. The preliminary requirement is to maintain the formation for a minimum of 60 s, despite any external disturbances.

This paper presents the modelling and simulation of a full-scale reusable launch vehicle and a towing aircraft attempting the formation flight for IAC. First, a suitable aircraft configuration is selected based on the aerodynamic performance of the selected test rocket stage. Important subsystems are identified and modelled comprehensively. Then, trajectory simulations are performed to identify the best approach and conditions for the formation. The sensitivity of the formation flight to critical factors like the idle thrust and wake turbulence from the towing aircraft are also analysed. The simulation showed that the minimum duration of formation flight could be maintained in the presence of external disturbances. Lastly, potential improvements and future simulations are discussed.

1. Introduction

Reusable Launch Vehicles (RLVs) have been a matter of interest ever since the 1970s. The peak of this research gave rise to the first operational RLV – The Space Shuttle [1]. Although widely successful, the Space Shuttle could not achieve the cost benefit of reusability due to the large refurbishment costs and lower launch frequencies following the loss of crew [2]. The early experience of reusability from RLVs like Space Shuttle and Buran demonstrated many challenges of finding a viable operational and business case for reusable launch systems. However, the recent success in development and operation of multiple reusable launch systems has become vital for reduction of launch costs and increase in launch frequencies. The cost of delivering cargo to the International Space Station (ISS) today is reduced by a factor of 4, when compared to the Space Shuttle era [3].

The reusable launch systems can be categorised into two types - Vertical Take-Off Vertical Landing (VTVL) and Vertical Take-Off Horizontal Landing (VTHL). Pioneering companies like SpaceX and Blue Origin use VTVL based RLVs [4]. However, the currently employed VTVL techniques, namely Return-To-Launch Site (RTLS) and Down Range Landing (DRL) require significant amount of fuel during descent.

The VTHL based winged RLVs can only glide back when sufficient energy is available [5]. For larger launchers, this would require descent from an orbit. Fly-Back Boosters (FB), which is a VTHL system powered by turbofans, also requires an additional propulsion system, adding to its inert mass [5]. In view of these challenges, an innovative approach called 'In-Air-Capturing (IAC)' was proposed and patented by DLR [6]. In this approach, a winged-rocket stage is captured mid-air using an aircraft and towed back to the launch site for horizontal landing.

A similar approach called Mid-Air Retrieval (MAR) has also recently emerged among many innovative launcher recovery concepts. Here, the reusable parts of the launcher are first slowed

* Corresponding author.
E-mail address: sunayna.singh@dlr.de (S. Singh).

https://doi.org/10.1016/j.jsse.2022.09.005

Please cite this article as: S. Singh, S. Stappert, L. Bussler et al., Full-scale simulation and analysis of formation flight during in-air-capturing of a winged reusable launch vehicle, Journal of Space Safety Engineering, https://doi.org/10.1016/j.jsse.2022.09.005

Acronyms/Abbreviations

3STO	Three Stage To Orbit
3DOF	Three Degrees of Freedom
6DOF	Six Degrees of Freedom
AoA	Angle of Attack
C3H8	Propane
CoG	Centre of Gravity
CFD	Computational Fluid Dynamics
DLR	German Aerospace Center
DRL	Down Range Landing
EOM	Equations of Motion
ELV	Expendable Launch Vehicle
FB	Fly-Back Boosters
FPA	Flight Path Angle
GG	Gas Generator
GLOW	Gross Lift-Off Weight
GTO	Geostationary Transfer Orbit
IAC	In-Air-Capturing
ISS	International Space Station
L/D	Lift-to-Drag
LH2	Liquid Hydrogen
LOX	Liquid Oxygen
MAR	Mid-Air Retrieval
MECO	Main Engine Cut Off
RANS	Reynolds-Averaged Naviers Stokes
RLV	Reusable Launch Vehicle
RP-1	Rocket Propellant-1 (Kerosene)
RTLS	Return-To-Launch Site
SC	Staged Combustion
TA	Towing Aircraft
THS	Trimmable Horizontal Stabilizers
TSTO	Two Stage To Orbit
VTVL	Vertical Take-Off Vertical Landing
VTHL	Vertical Take-Off Horizontal Landing

down using lifting devices like parachutes or parafoils and then, captured using a helicopter. Multiple launcher companies like Khrunichev from Russia [7], ULA from the USA [8] and Rocket Lab from New Zealand and USA [9] have invested into study and development of the technology. On May 2nd, 2022, Rocket Lab achieved the capture of the first stage of their launcher, Electron, using MAR. The stage was released by the helicopter shortly after the capture, to splash down in the ocean. A full recovery and subsequent operational use are yet to be demonstrated [9].

According to [7], the MAR approach can provide budget savings up to 30%, when compared to launch costs of Expendable Launch Vehicles (ELVs). However, the technology is limited by the size and mass of the rocket stages to be captured. The limitations of parachutes and helicopters also add to the constraints [10]. For these reasons, ULA switched their business case from MAR recovery of the large first stage of Vulcan launcher to only the partial recovery of its engine [8]. The IAC recovery approach can provide more flexibility that MAR because the size of the aircraft can be chosen based on the size and mass of the rocket stages. Additionally, IAC is estimated to provide a launch cost reduction of up to 35% assuming 15 launches per year. A detailed overview of the cost model and comparison with other RLV return modes can be found in [11].

Beyond the spaceflight regime, technological similarities have also been observed in aeronautical applications. The formation flight manoeuvre and capturing device in IAC are comparable to the technology seen in aerial refuelling [12]. Furthermore, on October 2021, the DARPA funded program X-61A Gremlin demonstrated a successful in-air recovery of X-61 UAV by C-130 cargo aircraft [13]. The project is aimed at the deployment and later recovery of a large number of small swarming drones.

1.1. Performance impact

Any RLV mode of operation (compared to an ELV) tends to degrade the launcher's performance due to the added stage inert mass or required descent propellant. However, the degree of performance degradation varies significantly depending on the mode of operation or separation conditions. Although a precise estimation of RLV costs is unattainable, the performance impact can provide a sound indication of the potential of different RLV return modes [14].

The performance impact of an RLV can be directly related to its ascent inert mass ratio or net-mass fraction, assuming that the engine specific impulse is not considerably affected. The inert mass ratio can be used as a direct indicator of performance since it can be directly related to the mass fraction used in the Tsiolkovsky (Rocket) equation. The inert mass of the stage ($m_{i,\,inert}$) during ascent flight consists of its dry mass and its total residual propellants including the propellant needed for controlled re-entry, landing or possible fly-back. The inert mass ratio (ς_i) is defined as:

$$\varsigma_i = \frac{m_{i,\,inert}}{m_0} \tag{1}$$

Where m_0 stands for Gross Lift-Off Weight (GLOW) of the RLV stage. The higher the inert mass ratio of a stage, the lower would be its acceleration performance when the propellant type and engine performance are kept constant. For a better understanding of the rocket design, the Structural Index (SI) is defined as,

$$SI = \frac{m_{dry}}{m_{propellant}} \tag{2}$$

Here, m_{dry} stands for the dry mass of the system and $m_{propellant}$ stands for the total propellant mass. The SI provides an indication for the lightness of the structural design and the amount of propellant that can be carried by the rocket.

Fig. 1 presents a comparison of the inert mass ratio and SI for generic Two Stage To Orbit (TSTO) launchers using different return modes of the reusable first stage (generated using Eqs. (1), (2)). All launchers have been sized for a Geostationary Transfer Orbit (GTO) of 250 km x 35786 km x 6° and a payload of 7.5 tons. They are analysed with different types of propellants (LOX-LH2, RP-1, LOX-CH4, LOX-H2 and LOX-C3H8) as well as different propellant loading based on the fuel required to reach target orbit and return [14]. As the mission and number of stages are identical, the inert mass ratio and SI can be represented as a function of total ascent propellant loading. Two types of engine cycles – Gas Generator (GG) and Staged Combustion (SC) have been used for the analysis.

It can be observed from Fig. 1 that the IAC mode provides the lowest inert masses across different propellant types when compared to FB mode, which requires a turbojet to fly back and the DRL, which requires propellant to land. The corresponding ascent propellant required for the mission is also smaller with IAC. On comparison of SI, it can be observed that the values for IAC remain lower than FB but higher than the VTVL methods across all propellant types. This is because both VTHL systems are equipped with wings and other additional systems (like landing gear), which add to the structural mass of the system. The SI for FB is the highest because the return mode requires an additional propulsion system for the descent.

Although VTVL systems are structurally lighter, they need to carry extra propellant for the descent. These return modes are then required to accelerate the extra propellant mass to reach the desired Δv, leading to higher inert masses and hence, decreased performance. Since the propulsion system for IAC is provided exter-

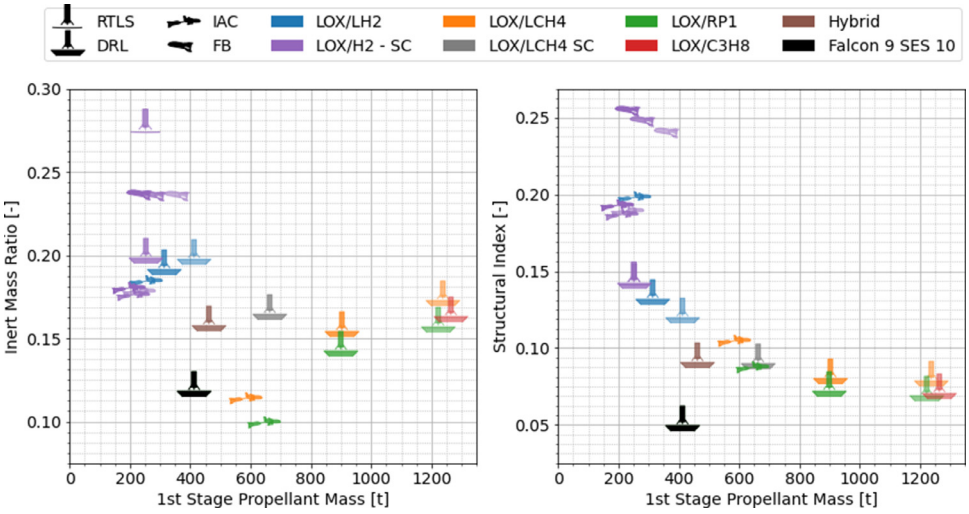

Fig. 1. Performance impact of different RLV return modes: inert mass index (Left) and structural index (Right).

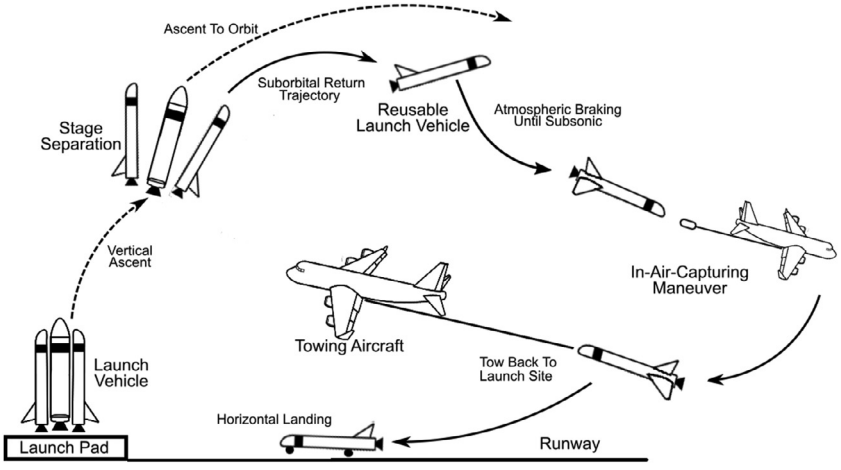

Fig. 2. A schematic of IAC mission cycle.

nally by an aircraft, the need for extra descent propellant is eliminated from the rocket design. Therefore, IAC has a potential for both mass and cost reduction and should be examined in further detail. A detailed comparative study of different RLV modes can be found in [14]. It must also be mentioned that the application can not only be used for partial or complete recovery of launch vehicles but also for smaller parts like fairings.

1.2. Mission Profile

The complete (generic) mission cycle of IAC is shown in Fig. 2. The process starts with a vertical launch from the launch pad. At Main Engine Cut Off (MECO), the winged first stage separates from the launch vehicle and the second stage moves on to the orbit. The first stage then begins a ballistic re-entry such that its velocity is reduced from supersonic to subsonic through atmospheric braking. In the meantime, a Towing Aircraft (TA) loiters at approximately 10 km altitude until the RLV is in the vicinity. Then, between an altitude of 2 km and 8 km, the TA approaches the RLV to form a gliding parallel formation. During this manoeuvre, a capturing device is released from the TA, which autonomously connects the two bodies via a rope. Finally, the RLV is towed back to an airstrip where it lands horizontally [5].

In this paper, the first sector of the IAC mission profile called the formation flight phase is examined using full-scale test cases. To achieve a parallel formation, the altitude, velocity and Flight Path Angle (FPA) of the RLV and the TA need to be comparable. To achieve this, both vehicles are required to have comparable aerodynamic performance. Therefore, in Section 2, the test cases are introduced and their aerodynamic performance is analysed using empirical methods. The most suitable configurations are selected and further analysed using CFD. Other important aircraft properties like the mass and flight envelope during the formation flight are also studied in Section 2. In Section 3, the simulation model is explained. Critical subsystems like propulsion, aerodynamics and control system are discussed in detail. The external disturbances originating from the wake of the aircraft are also analysed here. This is followed by the results in Section 4, wherein the formation flight simulations are presented. Sensitivity to some important aspects like idle thrust and wake disturbances is also examined here. The preliminary formation time achieved in this phase will be used as the target time for the capturing device to reach the RLV in future iterations. Finally, the paper is concluded in Section 5, and the planned future work is presented.

2. Selected Configurations for Formation Flight

The parallel formation for IAC requires both the participating vehicles to be in a gliding flight with similar altitudes, velocities and FPAs separated by a safe distance. One critical aspect to ensure

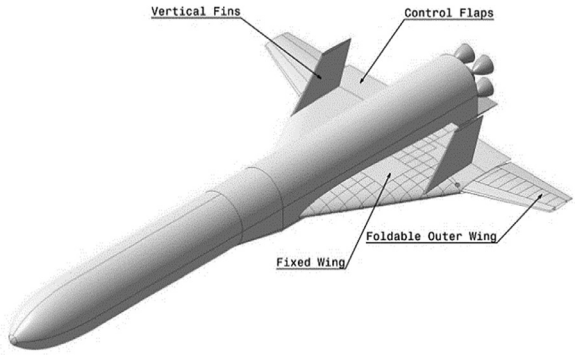

Fig. 3. Subsonic configuration of RLVC4 [17].

Fig. 4. Commercial airliner: A340–600 [18].

such a formation is that the aerodynamic performance of both the RLV and TA should be closely matched.

Typical winged re-entry vehicles have a maximum Lift to Drag (L/D) ratio between 2-4.5 in subsonic regime, as documented by Saltzman [15]. On the other hand, long range commercial aircraft can reach a L/D ratio of up to 20 [16]. Therefore, to reduce this gap in aerodynamic performance and prepare the vehicles for a successful formation, careful design selection and alterations may be required. In the coming section, the chosen full-scale test cases are presented. The aerodynamics of the chosen vehicles are analysed to identify any modifications that may be required for the formation flight. Further important characteristics, such as the mass and the flight envelope of the vehicles are presented.

2.1. Full-Scale Vehicles

2.1.1. Reusable Launch Vehicle (RLV)

For the current research, the RLV is selected to be the first stage of a 3 Stage-To-Orbit (3STO) launch vehicle proposed in [17]. This returning winged stage called RLVC4-IIIB has a special swept wing configuration. The outer wings of the spacecraft are folded in during the hypersonic re-entry to avoid shock-shock interaction [19]. Once the vehicle has slowed down to subsonic velocity, the outer wings are deployed (or unfolded) as shown in Fig. 3. The larger wings facilitate a higher trimmed L/D ratio of up to 6 in the subsonic regime, making the configuration suitable for IAC. Here, the term trimmed is used to define longitudinal stable configuration, such that there is no rotation about the Center of Gravity (CoG) of the vehicle. Control flaps are used for trimming and maneuvering, which can deflect up to $\pm 20^{\circ}$. During the descent, the RLV is expected to weigh 79,182 kgs. Other variants of the RLV can also be used for IAC and are given in [20].

2.1.2. Towing Aircraft (TA)

Based on the scale of the RLV, a suitably sized TA must be selected. The aircraft must support the drag from the RLV during the tow back to launch site. To achieve this, the TA should have sufficient payload and propulsion capability. Additionally, the aircraft should be accessible at low cost to minimize the cost of recovery.

For the current application of capturing a large RLV (approximately 80 tons), an Airbus A340-600 (shown in Fig. 4) is chosen [14]. The retired long-range jetliner has a large loading capacity and can support a payload of up to 68 tons. Its four Rolls Royce Trent 556 engines can provide a maximum continuous thrust of 197 kN each. Although the engines are kept in idle mode (minimum throttle setting) during the formation glide, they become critical in the following phases of IAC. Once the RLV is captured, these engines are required to throttle up and help the connected configuration gain altitude and reach suitable cruise conditions. A detailed study of this pull-up maneouvre and the required engine performance is presented in [21].

In studies performed in [22] and [23], it was found that repurposing flight-proven second-hand aircraft could facilitate lower recovery costs for IAC. The cost of acquiring the aircraft played a direct role in overall cost of recovery. Further, considering a maximum of 30 to 40 launches per year, the additional maintenance and costs originating from operating older engines did not contribute significantly to the overall operating costs. It was concluded that retired fleets like Airbus A340 and Boing 747 offered the best fit for IAC.

2.2. Aerodynamics

The cruise L/D ratio for a typical aircraft from the A340 family can reach up to 19.3 [16]. However, for the capture of RLVC4-IIIB using IAC, the desired L/D ratio is close to 6. Therefore, some additional drag sources must be included to lower the L/D ratio of the TA. Drag can be generated using the existing control surfaces, like the spoilers and also, other components such as landing gear. According to the Airbus Maintenance manual [24], an A340-600 consists of three sets of landing gear:

- Two main landing gears with four-wheel assembly that are located under the wing and retract sideways towards the fuselage.
- A centreline landing gear with four wheels that is located at the belly of the aircraft and retract forward.
- A nose landing gear with twin wheels that retracts forward below the cockpit.

Additionally, the spoilers can be deflected up to -30° for the speed brake function. However, to consider some room for manoeuvrability, deflection of only up to -20° is considered. To find the configuration with the closest L/D ratio to the chosen RLV, different TA configurations are analysed using empirically generated aerodynamic datasets as presented in Table 1.

The empirical methodology used for the analysis, is based on Digital DATCOM methods [25]. The DLR tool called CAC, estimates the longitudinal aerodynamic coefficients for a range of flight points (defined by altitude and Reynolds number) as a function of Angle of Attack (AoA) and Mach number. The geometry of the aircraft is defined using airfoil surfaces and simple geometric shapes representing different components. The lifting line theory is used to predict the aerodynamic properties of the wings [26]. The aerodynamic contributions from individual components are then combined to get the final estimates. The static stability and trimming requirements from control surfaces can also be estimated using the tool.

The maximum L/D ratios (at AoA $= 8^{\circ}$) of different TA configurations at Mach 0.45 are presented in Table 1. Two potential configurations (TA4 and TA5) provide a close match to the target L/D of 6. It can be observed from the data, that deploying the landing gear can bring down the L/D of the aircraft considerably. However, deploying the landing gear mid-flight can lead to structural vibrations and add to the flow disturbances. Since TA4 uses only two sets of landing gear compared to TA5, which uses all three sets, it is likely to cause smaller disturbances. Further, the centreline landing gear can be removed to house the capturing device in the bay

Table 1
Analysis of aerodynamic performance for different TA configurations using empirical methods.

	Description	MaximumL/D ratio
TA1	Clean Configuration	19.36
TA2	Spoilers −20°	12.97
TA3	Front Landing Gear Deployed, Spoilers −20°	10.02
TA4	Front and Main Landing Gear Deployed, Spoilers −20°	6.25
TA5	All Landing Gears Deployed, Spoilers at −20°	4.78

Table 2
Simulation flight point for RANS [27].

Parameter	Value
Velocity [m/s]	142.39
Mach	0.45
Altitude [m]	6000
Pressure [Pa]	47,248.92
Density [kg/m^3]	0.66065

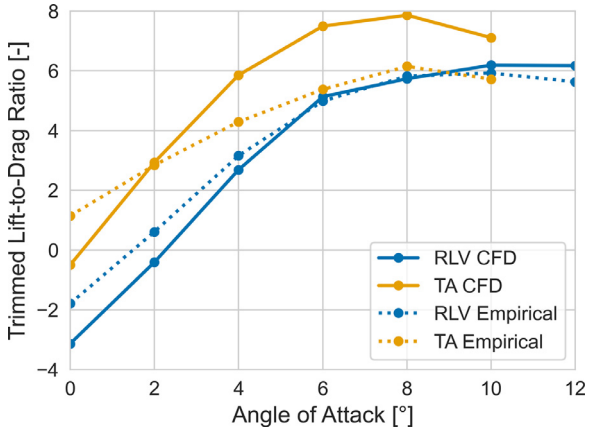

Fig. 5. Aerodynamic performance of RLV and TA.

and provides close access to the structural elements near the aircraft CoG for the distribution of towing loads. Therefore, TA4 is selected to be the most suited configuration.

The aerodynamics of TA4 and RLV configurations are further analysed using Reynolds-Averaged Naviers Stokes (RANS) to achieve high confidence datasets. The CFD simulations are performed using the open source code OpenFOAM v6.0. Both vehicles are analysed at the flight point shown in Table 2. Since the flight point exists in the compressible subsonic flow regime, the rhoSimpleFoam solver is selected. The k-ω SST turbulence model is used to model the current flow areas [27]. A sensitivity study on mesh density is also performed to assure a computationally effective yet accurate grid resolution.

Fig. 5 shows the comparison of aerodynamic performance obtained using CFD and empirical estimates at the flight point in Table 2. It can be observed that the empirical estimates for the TA do not match the numerical results from CFD very closely. This is simply because complex geometries like landing gear are difficult to model accurately using empirical methods. The simpler wing-body-fin geometry of the RLV shows good agreement between empirical and CFD datasets. The selected TA configuration with spoilers deflected at -20°, front and main landing gears deployed reaches a maximum trimmed L/D ratio of 8 at an AoA of 8°. However, the RLV only reaches a maximum trimmed L/D ratio of 6 at an AoA of 10°. Although the performance is not identical, yet they may be similar enough to maintain a formation for some time. An extensive dataset is generated using the CFD data (presented in Section 3.2.1) and used in trajectory simulations of formation flight.

2.3. Mass Properties

The current full-scale scenario involves two sizable aircraft. The RLV descending with an unpowered glide is assumed to have a constant mass throughout the formation flight of approximately 80 tons. For the TA, the dive configuration is considered to have no payload and some parts, such as the central landing gear, removed. Depending on the required fuel for the trip, the aircraft is expected to weigh between 180 tons to 310 tons during formation flight. However, the mass of the aircraft also affects its aerodynamic behaviour. This effect can be observed with a sensitivity study performed using the 2DOF steady flight Equations of Motion (EOM) given as follows:

$$m\dot{V} = T + W\sin\gamma - D = 0 \tag{2}$$

$$mV\dot{\gamma} = L - W\cos\gamma = 0 \tag{3}$$

Here, V is the velocity in m/s, m is the mass of the aircraft in kg, L is the lift force in N, D is the drag force in N, T is the thrust in N, W is the weight of the aircraft in N and γ is the FPA in radians. For the study, it is assumed that the acceleration and the rate of change of FPA of the system remain zero. The thrust is assumed to act only in the direction of the velocity. The analysis is performed at the flight point given in Table 2. Eqs. (2), (3) are then statically solved for a range of masses between 180 tons and 310 tons, and the resulting values of AoA and FPA are studied.

Fig. 6 (Left) shows the effect of TA mass on the FPA. The corresponding AoA and L/D is plotted in Fig. 6 (Right). It can be observed that for larger TA mass, lower FPAs can be reached. Further, the L/D ratio is reduced with larger masses. Since a large AoA (up to 10°) can help slow down the aircraft during descent, a heavier configuration seems favourable. Also, a lower FPA may be required due to the RLV descending steeply (low L/D ratio). Based on these factors, a mass of 280 tons was selected to facilitate a longer formation time.

Further, the effect of idle thrust (10% engine throttle) is also shown in Fig. 6 (Left). Compared to unpowered descent, it appears that including idle thrust increases the FPA. As a result, the TA cannot descend as steeply and could lead to challenges during formation flight. A detailed analysis and modelling of idle thrust will be discussed in Section 3.3.

2.4. Flight Envelope

Since the aerodynamic properties of the vehicles are not exactly identical, the vehicles would have different flight envelopes. To identify the flight conditions for formation flight, the glide envelope of both the vehicles are analysed between the minimum (-10°) and the maximum (0°) expected FPAs. It is also critical to analyse the envelope to establish safe or unsafe flight profiles (for instance, to avoid stall).

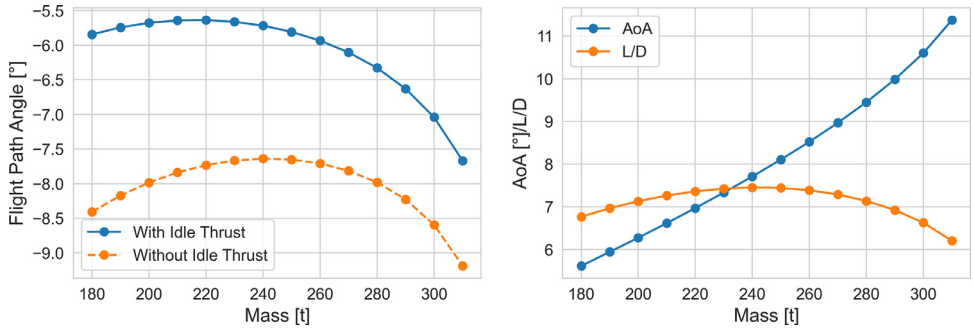

Fig. 6. Sensitivity of TA aerodynamics to mass.

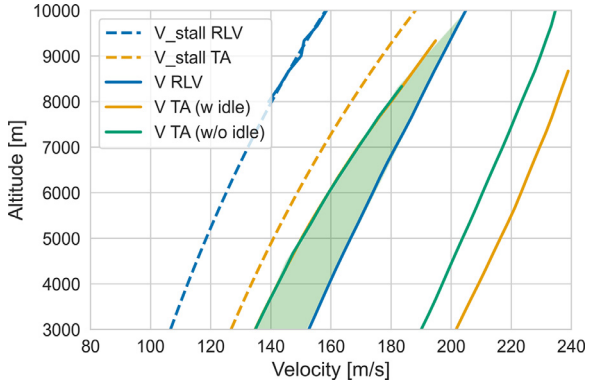

Fig. 7. V-h flight envelope for formation flight.

Aircraft stall typically occurs at high AoAs around 15° [28]. However, the exact stall region varies from one aircraft to another, and is dependent on the aircraft aerodynamics. The stall limits of the A340-600 in its original configuration is expected to be different from the configuration used during formation flight. Since the aerodynamic dataset was generated for a smaller AoA range (0° to 10° for TA and 0° to 12° for RLV), the exact stall conditions could not be reached within this range. The flight envelope is then computed using Eqs. (2), (3) stated in the previous section. Again, it was assumed that the acceleration and the rate of change of FPA of the system are zero and the thrust acts only in the direction of velocity.

Fig. 7 shows the height-velocity diagram (or h-V curve) for the expected FPA range of formation flight. The highlighted green region indicates the operating altitude and velocity in which the flight envelopes of the two vehicles overlap. In these flight conditions, the formation flight can be maintained. For this analysis, the highest AoA of the aerodynamic dataset (10° for TA and 12° for the RLV) are assumed as stall AoAs to establish safety margins. An important observation that can be made from the figure, is that the formation envelope occurs within the safety limits (between solid lines) of each vehicle. This indicates that there is no risk of stall within the AoAs required during formation flight.

3. Modelling of Subsystems

For a realistic simulation of the full-scale scenario of IAC, some important subsystems must be reliably modelled. The dynamics of the vehicles not only depend on the aerodynamics, but also other factors like the environment, propulsion system and external disturbances. Further, a simplified flight controller is required to ensure that the formation is maintained as long as possible.

For the current study, only 3DOFs are analysed. The translational motion is restricted to X and Z-directions (no sideslip) and the rotational DOF is restricted to pitch. Fig. 8 shows the framework of the plant model used for closed loop simulation of the formation flight trajectory. In the coming section, the modelling of these three critical subsystems and the control architecture are presented.

3.1. Environment Model

The environment model defines the external factors that affect the dynamics of the system. First, the elliptical planet block uses the "U.S World Geodetic System 1984 (WGS84)" to define the gravitational acceleration, based on the position of the vehicle with respect to Earth [29]. The model considers the change in gravitational acceleration due to Earth's rotation and irregular shape.

Next, the atmosphere module uses the US Standard Atmosphere (US76) to determine the pressure, density and temperature of the air based on the altitude of the vehicle. These parameters further affect the properties of the air flow, such as the Reynold's number, dynamic pressure and free stream velocity.

The wind/ wake module is used to include the effect of external disturbances on the vehicle trajectory. For the current study, the wake from the aircraft plays a critical role in the dynamics and is analysed in further detail.

3.1.1. Aircraft Wake

The formation flight requires the RLV to be in close proximity behind the TA (about 350 m for the current test scenario). This means that the aircraft wake can act as a disturbance to the RLV and may lead to loss of formation. Therefore, RANS calculations for the wake were performed for A340-600 with the spoilers at -20° and the front and main landing gears deployed. The same simulation parameters given in Section 2.2 were used for the wake. A detailed description of the CFD study of the wake can be found in [27].

Fig. 9 shows the velocity contour plots, wherein the effects of wake can be seen as far as 315 m from the nose of the aircraft. The wake behaviour is also varied with AoA and the effects can be observed more distinctly in Fig. 10. The figure shows the wake velocity components in streamwise direction (horizontal) and downwash direction (vertical) as a function of distance from the aircraft. While the magnitude of the streamwise velocity (U_X) for both 0° and 8° AoA remain similar, a drift in the Z-direction can be observed for 8° AoA. Then, it appears that the magnitude of downwash component (U_Z) is strongly affected by the AoA of 8°. This is evident by the fact that even after moving away from the TA, the downwash velocity component remains close to 8% of the free stream velocity (U_∞). The change in velocity caused by this component can possibly affect the AoA of the RLV leading to a disturbance in formation. Thus, it is critical to analyse the sensitivity of the formation flight trajectory to the wake disturbances.

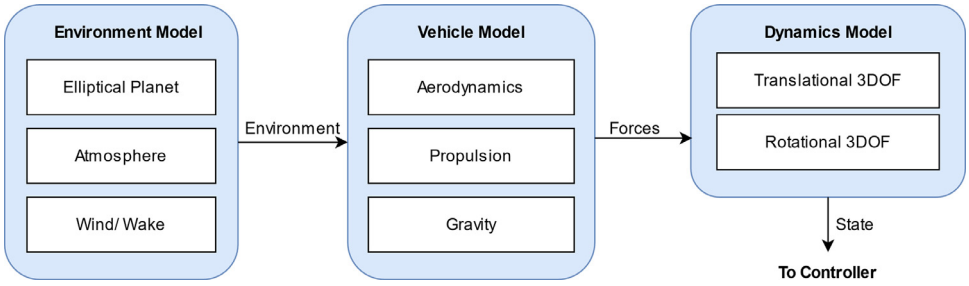

Fig. 8. Plant model for formation trajectory simulation.

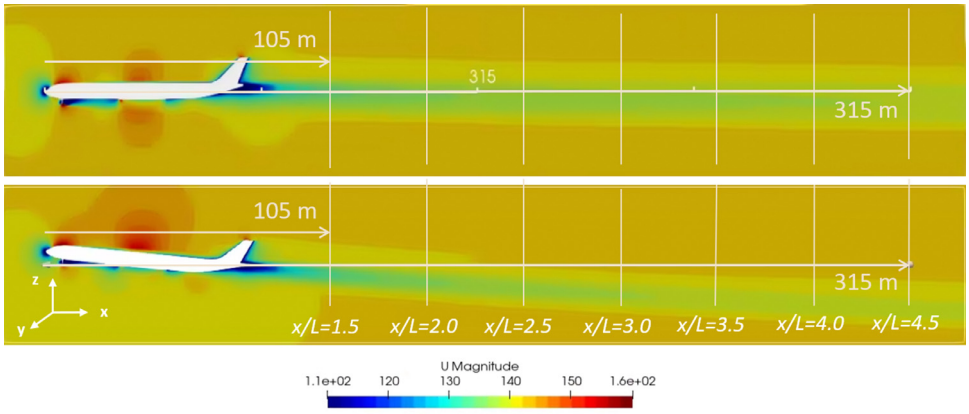

Fig. 9. Wake velocity magnitude contours for AoA of 0° (top) and 8° (bottom).

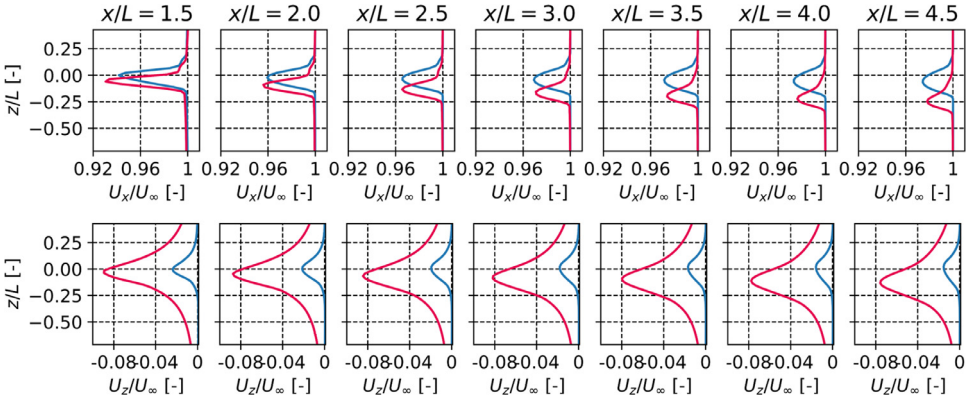

Fig. 10. Wake Profiles in the Fuselage Plane for 0° (blue) and 8° (red) AoA; Streamwise Velocity Component (top) and Downwash Velocity Component (bottom).

Another important parameter derived from the CFD study, is the turbulent kinetic energy (k). This factor is associated with the eddies in turbulent flow and can be used to model the velocity fluctuations in the wake [30]:

$$u' = \sqrt{\frac{1}{3}\left({u'_x}^2 + {u'_y}^2 + {u'_z}^2\right)} = \sqrt{\frac{2}{3}k} \tag{4}$$

Here, u' is the root mean square of velocity fluctuations (u'_x, u'_y, u'_z) due to turbulence. It must be stated that the CFD simulations were performed using a steady state solver (rhoSimpleFoam). Thus, the turbulence approximation is rather simplified compared to the complex turbulence patterns typically observed in wake. However, for the current study the simplified model provides sufficient representation of wake.

The wake module for simulation consists of look-up tables, which output a change in free stream velocity based on the position of the RLV behind the aircraft. Time dependent velocity fluctuations are added to this data to represent turbulence using Eq. (4). This change in velocity is then added to the free stream velocity of the airflow. The RLV sees a turbulent flow due to the changing airspeed, which leads to further disturbances in its AoA. The module is only used for the RLV, which is expected to be affected by the aircraft wake.

3.2. Vehicle Model

The vehicle model consists of all the systems that are intrinsic to the aircraft design. It accounts for the forces that affect the dynamics of the system. The gravity module computes the force due to the weight of the vehicle. The aerodynamics and propulsion models require a larger dataset dependent on the flight conditions. They are explained in further detail.

3.2.1. Aerodynamics

For the trajectory simulations, the CFD generated aerodynamic data at Mach 0.45 (shown in Fig. 5 and explained in Section 2.2), is extended across the subsonic regime (Mach 0.3 to Mach 0.75)

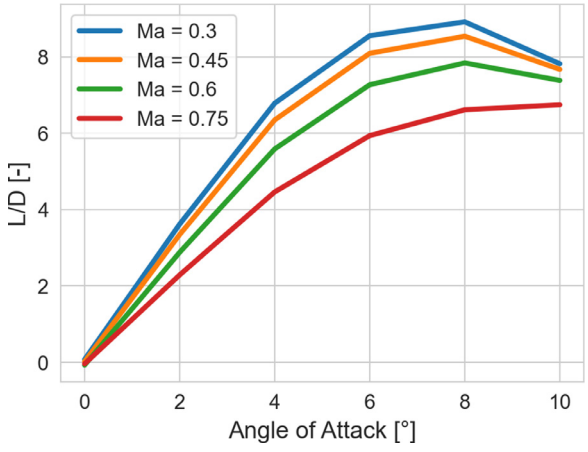

Fig. 11. Extended aerodynamic performance of TA.

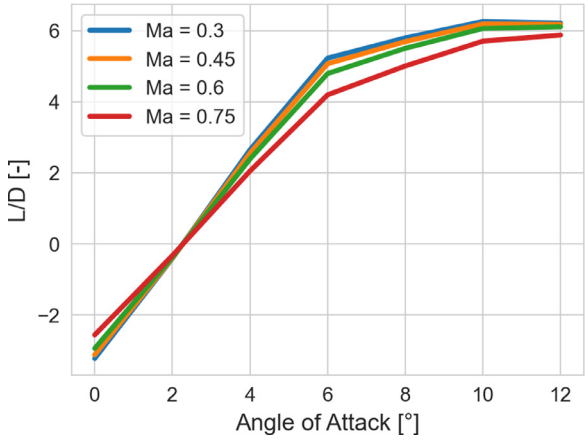

Fig. 12. Extended aerodynamic performance of RLV.

using empirical relationships. The lift coefficient (C_L) and pitch moment coefficient (C_M) are extended using Prandtl-Glauert compressibility correction [26]. The total drag coefficient (C_D) from CFD can be split into zero-lift drag and lift induced drag. This is used to derive the zero lift drag (C_{D0}) and k value and the data is extended using the drag polar relationship to different Mach numbers [26]:

$$C_D = C_{D0} + k.{C_L}^2 \tag{5}$$

The k *in* Eq. (5) is a constant that depends on the wing aspect ratio and is assumed to be fixed for the wing design. The resulting extended aerodynamic performance for the TA and RLV is shown in Fig. 11 and Fig. 12 respectively. Finally, the effect of control surface deflection is added using the estimates from the DLR tool CAC (mentioned in Section 2.2). The complete aerodynamic dataset is added to the simulation model using look-up tables (in Simulink) as a function of Mach number, AoA and control surface deflection.

3.2.2. Propulsion

For the current study, the A340-600 consists of four Rolls Royce Trent 556 engines. These high-bypass turbofan engines provide a maximum take-off thrust of 260 kN and a maximum continuous thrust of 197 kN each [31]. For the formation flight, the TA needs to be in a gliding descent. Typically for commercial airliners, the engines are not completely turned off and kept in idle mode (the minimum throttle setting) during a gliding descent. For a jet engine, the flight idle RPM varies between 45% to 60%, depending on the manufacturers design [32]. This corresponds to a throttle value between 10% to 20%. For the current study, a throttle value of 10% is assumed as idle.

Since idle thrust acts against the drag, it would lead to a different descent rate than a completely unpowered glide. It could make formation flight more challenging. The effect of idle thrust on aerodynamic angles can be seen in Fig. 6, wherein the achievable FPAs with idle thrust are much larger than the FPAs without idle thrust. Thus, to ensure longer formation time, it is worthwhile to examine the trajectories without idle thrust. The possibility of turning off two engines (5% idle) can also be considered. Therefore, the formation flight trajectories are examined for sensitivity to idle thrust.

It must be stated that idle thrust is mainly used in commercial airliners for the safety of passengers and to power some electrical systems. Since the engine cannot be throttled up quickly in case a sudden manoeuvre is required, the aircraft being on idle provides more resilience to the pilot. Additionally, turning off engines can increase the drag substantially, which may increase the risk of stall. Nonetheless, it is possible to shut down and restart the engines mid-flight, as long as the flight is within the operating envelope [33].

Another aspect that cannot be overlooked while modelling the propulsion is that the thrust for airbreathing engines varies with air density. For any fixed throttle setting, the thrust produced at lower altitudes is higher than thrust produced at higher altitudes. This is because the air density is higher close to the Earth. The relationship is included in the model using a basic formula [34]:

$$T = T_{SLmax}\delta_T\left(\frac{\rho}{\rho_{SL}}\right) \tag{5}$$

Where T_{SLmax} is the maximum thrust at sea level in N, δ_T is the throttle setting of the engine, ρ is the air density at the current altitude in kg/m^3 and ρ_{SL} is the air density at the sea level in kg/m^3. The resulting values from Eq. (5) provides an estimate of the variation in thrust due to change in altitude.

3.3. Dynamics Model

The dynamics model contains the EOMs of the aircraft in 6DOF. The module consists of three translational EOMs and three rotational EOMs that are defined using Newton's second law (assuming rigid bodies and constant mass) [29]. The translational EOMs are defined by:

$$\bar{F} = \frac{d(m\bar{v})}{dt} \tag{6}$$

Where $\bar{F}$ is a vector containing the forces (X, Y and Z directions) in N, $\bar{v}$ is the velocity vector of the vehicle in m/s and m is the mass of the vehicle in kg. The rotational EOMs are defined by:

$$\bar{M} = I\frac{d(\bar{\omega})}{dt} + \bar{\omega} \times I\bar{\omega} \tag{7}$$

Where $\bar{M}$ is a vector containing the moments (X, Y and Z directions) in Nm, $\bar{\omega}$ is the angular velocity vector of the vehicle in rad/s and I is a 6×6 matrix representing the inertia tensor of the vehicle. Detailed explanation of the equations can be found in [29]. Although, the Eqs. (6), (7) are set up for 6DOF, only 3DOF are studied in the current research. Due to the limited aerodynamic dataset, only two translational DOF (X and Z) and one rotational DOF (pitch) are considered. Since there are no aerodynamic forces and moments in the other 3DOF, the dynamics are reduced.

3.4. Controller Architecture

For a successful and prolonged formation flight, the altitude and velocity of the vehicles should be matched closely. Since the

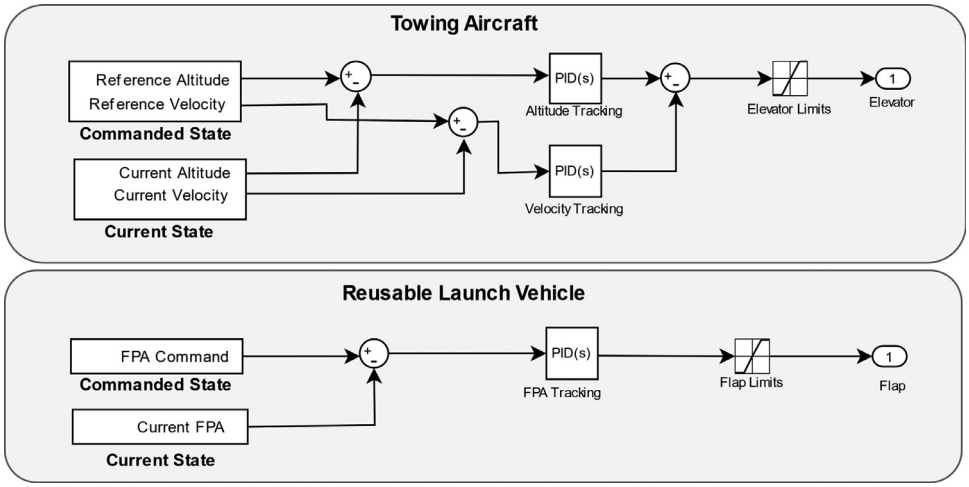

Fig. 13. Flight controller architecture for formation flight.

aerodynamic performance of the two vehicles are slightly different, a controller is required to maintain the best possible trajectory for the formation flight. For this study, a simple flight controller (shown in Fig. 13) is set up. Both vehicles are controlled independently using PID controllers. The RLV is commanded to fly with a constant FPA of -8° (based on the limit of flight envelope). The TA is commanded to follow a predefined reference trajectory of RLV with a constant FPA of -8°. Since the TA is faster than RLV and cannot fly very steep due to a higher L/D ratio, PID controllers are set up to find the best balance between altitude and velocity. Due to the different aerodynamic properties of the two vehicles, matching the FPAs result in different altitude and velocity profiles. Hence, a FPA controller was not used for the TA.

The RLV is controlled and trimmed using flaps that can be deflected up to ±20°. The TA is trimmed using Trimmable Horizontal Stabilizers (THS), which can be deflected between -14° and +2°, and the elevons or elevators that can be deflected between -30° to +15° are used for rapid manoeuvring. The sensors and actuators are assumed to be ideal for the study.

4. Results

Using the simulation model presented in Section 3, trajectory simulations are performed. To get a better understanding of the formation flight phase, the sensitivity of the trajectory to important factors like idle thrust and external disturbances from the wake of the aircraft is analysed. The criteria or constraints for formation are defined as follows:

- The formation flight must be achieved between an altitude of 3000 m and 8000 m.
- The RLV should remain behind the TA throughout the formation.
- The relative distance between the TA and RLV should be maintained between 70 m to 350 m.
- The relative velocity between the TA and RLV should not exceed ±3.5 m/s.
- The relative altitude should be maintained between ±150 m.
- The control surfaces should be unsaturated to allow room for manoeuvrability.

The vehicles are considered to be in formation when all the stated criteria are met. A preliminary requirement for 60 s of formation flight is considered. This criterion is established as a safety margin. In case of an abort scenario where the vehicles are 200 m apart and moving with a relative velocity of 3.5 m/s, a minimum of 60 s would be required to perform collision avoidance maneouvres and avoid loss of vehicles. Additionally, from preliminary simulations of capturing device given in [35], the capturing device was able to perform up to two maneouvres spanning up to 30 m in the YZ plane within a span of 60 s. The initial criteria are preliminary and will be reiterated in future work.

4.1. Formation Trajectory without Idle Thrust

The formation flight trajectory is first analysed without idle thrust. The initial conditions for the study are derived from a sensitivity study presented in [36]. Fig. 15 shows the altitude, velocity and relative distance between the RLV and TA during the formation. The highlighted green region marks the area in which the formation criteria is met. It can be observed that about 68 s of formation could be maintained. Even though the preliminary criterion of 60 s is met, challenges appear due to differences in aerodynamic properties. The TA cannot fly with a trajectory as steep (low FPA) as the RLV due to a higher L/D ratio. A longer formation can be achieved by adding further drag generating surfaces to the TA and will be examined in future iterations.

From Fig. 14, it can be seen that the control surfaces of the TA and the RLV remained unsaturated. This indicates that there is still scope for maneouvrability and the formation flight is mainly constrained by the aerodynamic performance of the vehicles.

4.2. Sensitivity Studies

Apart from the aerodynamics of the participating vehicles, the duration of formation flight also depends on factors like idle thrust of the aircraft engines and wake disturbances. Hence, the influence of these factors is studied in the following subsections.

4.2.1. Sensitivity to Idle Thrust

As it was addressed in Section 3.2.2, jet engines for commercial airliners are typically kept in idle mode for gliding. The idle thrust acting against the drag contributes to the performance of TA, thereby virtually increasing the performance gap between TA and RLV. For the formation flight, this could increase the challenges because matching the velocity and altitude at the same time becomes difficult. Since the A340-600 has four engines, the impact of idle thrust from fours engines (10% throttle) and two engines (5% throttle) are compared against the case when the engines are completely turned off (0% throttle).

Fig. 16 shows the effect of idle thrust on the FPAs observed during the formation flight. It can be observed that the TA is able

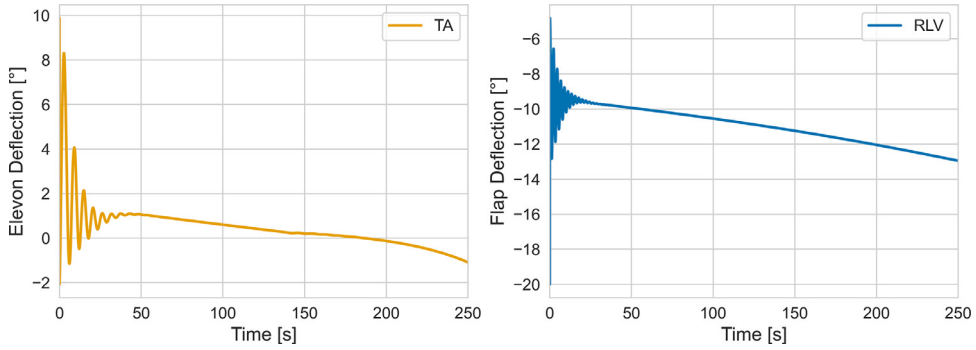

Fig. 14. Control deflections during formation flight: TA (Left) and RLV (Right).

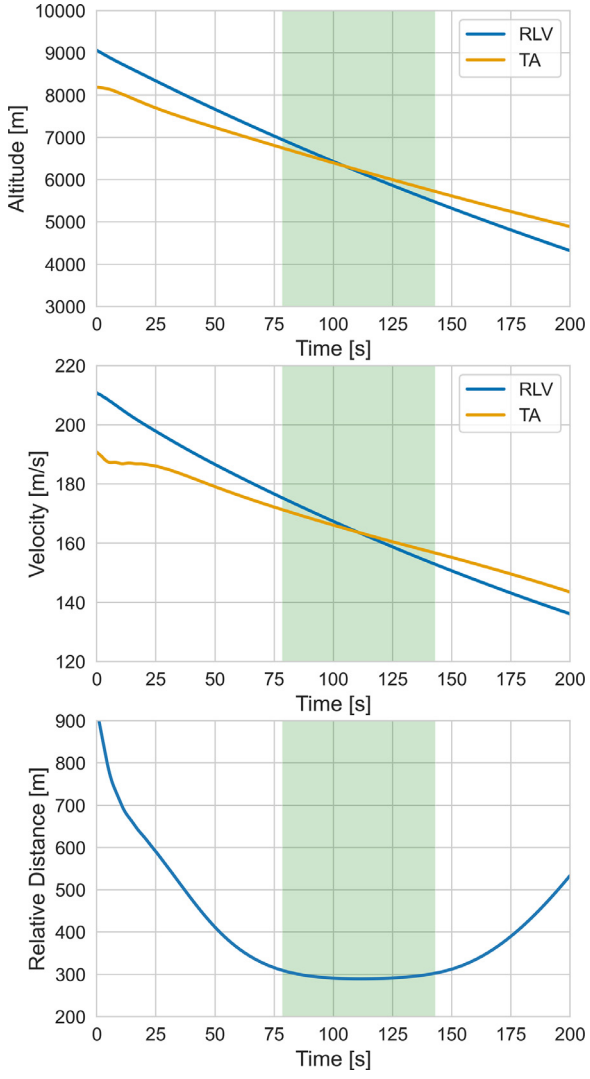

Fig. 15. Formation flight trajectory without Idle thrust.

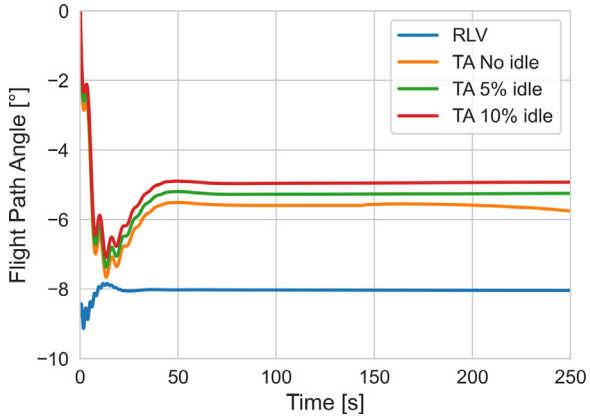

Fig. 16. Effect of Idle thrust on formation flight trajectory.

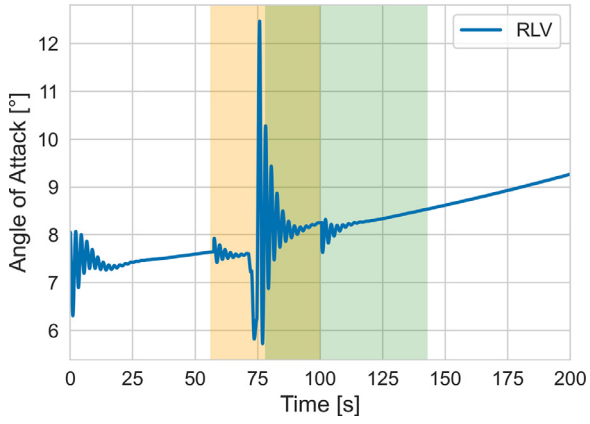

Fig. 17. Sensitivity of RLV AoA and formation flight trajectory to TA wake.

to descend steeper (lower FPA) when no idle thrust is considered. Adding the idle thrust from two engines (5% throttle) and four engines (10%) increased the FPA leading to less steep trajectories. This reduces the formation time as the altitude becomes more challenging to match. Based on the trajectory simulations, the formation time is reduced to 50 s with 5% throttle and 32s with 10% throttle. To conclude, when the idle thrust is considered the TA could not achieve at least 60 s of formation flight. However, when no idle thrust was included, longer formations of more than 60 s could be maintained.

4.2.2. Sensitivity to Wake Disturbances

As it was stated in Section 3.1.1, the aircraft wake at higher AoAs has a significant downwash component that can disturb the AoA of the RLV when exposed to it. For an AoA of 8°, this component was found to reach up to 11% of free stream velocity. Such a high deficit in vertical velocity can drastically disturb the formation and therefore, should be analysed.

Fig. 17 shows the effect of wake on the AoA of RLV. The time period in which the RLV was exposed to the wake is marked by the orange area, while the green area shows the duration of formation flight. It can be observed from the plot that substantial disturbance has been caused to the RLV AoA at the peak of wake exposure.

However, since the exposure to the most perturbing part of the wake is short, the formation is not broken. This can be explained better using Fig. 10, which shows the velocity components of the wake behind the TA. It can be seen from the figure that the region of highest velocity deficit is limited to a span of about 10 m. Since the RLV simply passes through it, the exposure is not prolonged and AoA is recovered to around 8° as shown in Fig. 17.

On comparing the formation time in Fig. 17 with the time in Fig. 15, it can be concluded that even though the formation is maintained with the wake, the overall duration of formation flight is slightly reduced (by 1.2 s) because of the wake disturbance. Nonetheless, the minimum requirement of 60 s of formation could still be maintained.

5. Conclusions and Future Work

A detailed investigation of formation flight in IAC is fundamental to understand the challenges and risks involved in the manoeuvre. This study is aimed at examining this phase through simulation and analysis of full-scale test cases. For this research, the two test vehicles are chosen to be RLVC4-IIIB, which is a large winged stage weighing approximately 80 tons and the A340-600, which is a retired long-range aircraft that can support the towing loads from the large stage. Since the formation flight requires both vehicles to have a similar velocity, altitude and FPA, their aerodynamic performances should also be similar. Therefore, a comparative study for different TA configurations is performed using empirical methods. It is found that the A340-600 configuration with spoilers deflected to -20°, and with front and main landing gear deployed is the most favourable option for the capture of RLVC4-IIIB.

Next, critical properties of the selected vehicles like aerodynamics, mass and flight envelope are analysed. RANS studies performed for the selected test cases concluded that the RLV has a maximum L/D ratio of 6 at an AoA of 10° and shows close agreement with the empirically data. The TA reaches a L/D ratio of 8 at the AoA of 8°. . A sensitivity study is then performed to analyse the effect of mass on the aerodynamics of the TA, and a final mass of 280 tons is selected for the formation flight. Next, the flight envelopes of both the vehicles are analysed. It is concluded that the vehicles do not reach stall within the envelope required for the formation glide.

The simulation model is then presented and the modelling of some important subsystems like aerodynamics, propulsion, wake disturbances and flight controller are explained in detail. A simplified model for airbreathing propulsion of TA is included by writing thrust as a function of sea-level thrust, throttle and air density, which changes with altitude. The role of idle thrust in jet engines is also examined and it was deduced that idle thrust (minimum throttle setting) increases the achievable FPA of TA, therefore preventing it from diving too steep. This would further make the formation flight more challenging. Next, RANS studies performed on wake showed that at higher AoAs, the vertical component of the wake could cause considerable disturbance. A simple PID architecture is used to follow a constant FPA of -8° for RLV. The TA also uses PID controllers to follow the velocity and altitude profile of the RLV trajectory.

The criteria for successful formation are set to be a relative distance less than 350 m, a relative altitude within ±150 m and a relative velocity within ±3.5 m/s for the two vehicles. From the 3DOF trajectory simulations, it was found that the 60 s formation could not be maintained when idle thrust was included. However, without idle thrust, a formation of up to 68 s could be achieved. But turning on engines again and bringing it to full throttle takes some time, and could add some operational risk in the next phases of IAC. This factor should be accounted for in the following simulations and consequent risks should be analysed. A sensitivity study to analyse the effect of external disturbances showed that the formation could be maintained despite disturbances from wake of the TA. The wake is found to significantly affect the AoA of the RLV due to the strong downwash component.

Future work will aim at extending the formation time by alternate methods. For instance, possibility of using flaps (used for speed braking during landing) can be explored. Performing drag inducing maneouvres like forward slip during formation flight can be studied. The preliminary criteria will be modified to more realistic constraints. The trajectory simulations will be extended to 6DOF and the effect of the 3D wake will be analysed in detail. Additional factors like sensor fusion, signal delay, noise etc. will also be included. Future simulations will include advanced control of the capturing device, attempting to capture the RLV when both vehicles are in formation flight. The capabilities of the capturing device to perform the maneouvre within a short formation flight will be studied in detail and further iterations will be performed accordingly. Finally, optimized trajectories as previously analysed in [37] and multiple failure scenarios will also be studied for IAC.

Declaration of Competing Interest

The authors declare that they have no known competing financial interests or personal relationships that could have appeared to influence the work reported in this paper.

CRediT authorship contribution statement

Sunayna Singh: Methodology, Software, Validation, Visualization, Formal analysis, Writing – original draft, Writing – review & editing. **Sven Stappert:** Formal analysis, Supervision. **Leonid Bussler:** Formal analysis, Supervision. **Martin Sippel:** Conceptualization, Supervision, Project administration. **Yakut Cansev Kucukosman:** Formal analysis, Resources. **Sophia Buckingham:** Formal analysis, Resources.

Acknowledgements

This work was performed under the Horizon 2020 project '**F**ormation flight for in-**A**ir **L**auncher 1st stage **C**apturing demonstrati**on**' (**FALCon**) aimed at development and testing of the "In-Air Capturing" technology. FALCon, coordinated by DLR-SART, is supported by the EU within the Programme 5.iii. Leadership in Enabling and Industrial Technologies – Space with EC grant 821953. Further information on FALCon can be found at http://www.FALCon-iac.eu

References

[1] A.R. Pielke, The rise and fall of space shuttle, Am. Sci. (2008) 432–434.
[2] D.R. Jenkins, Space Shuttle: Developing an Icon: 1972-2013, Specialty Press, 2016.
[3] H.W. Jones, N.A.S.A. Ames Research Center, The Recent large reduction in space launch cost, 48th International Conference on Environmental Systems, ICES-2018-81, Albuquerque, New Mexico, 2018 8-12 July.
[4] A. Marwege, A. Gülhan, J. Klevanski, C. Hantz, S. Karl, M. Laureti, G.D. Zaiacomo, J. Vos, M. Jevons, C. Thies, A. Krammer, M. Lichtenberger, J. Carvalho, S. Paixão, RETALT: review of technologies and overview of design changes, CEAS Space Journal 14 (2022) 433–445, doi:10.1007/s12567-022-00458-9.
[5] M. Sippel, J. Klevanski, Simulation of dynamic control environments of the in--air-capturing mechanism, 6th International Symposium on Launcher Technology, Munich, Germany, 2005 8-11 November.
[6] Patentschrift (patent specification) DE 101 47 144 C1, Verfahren zum Bergen einer Stufe eines mehrstufigen Raumtransportsystems, released 2003.
[7] S.V. Antonenko, S.A. Belavskiy, 'Mid-Air Retrieval technology for returning of reusable launch vehicles' boosters, Progr. Propuls. Phys. 1 (2009) 481494, doi:10.1051/eucass/200901481.
[8] M. Ragab, F.M. Cheatwood, F. M, S.J. Hughes, A. Lowry, Launch vehicle recovery and reuse, AIAA Space 2015 Conference and Exposition, Pasadena, 2015 31 August-2 September.

[9] Stephen Clark, Spaceflight now, rocket lab briefly catches booster in mid-air after successful launch, https://spaceflightnow.com/2022/05/03/rocketlabbrieflycatchesboosterinmidairaftersuccessful-launch/, 2022, (accessed 10 August 2022)
[10] M. Sippel, S. Stappert, S. Singh, RLV-return mode 'in-air capturing' and definition of its development roadmap, 9th European Conference for Aeronautics and Space Sciences (EUCASS), Lille, France, 2022 27 June –1 July.
[11] M. Sippel, S. Stappert, M. Simioana, Technical report on different RLV return modes performance, D2.1, FALCon Project Deliverable (2020) https://elib.dlr.de/137735/. (accessed 10 August 2022).
[12] P.R. Thomas, U. Bhandari, S. Bullock, T.S. Richardson, J.L. Du Bois, Advances in air to air refuelling, Progr. Aerospace Sci. 71 (2014) 1435, doi:10.1016/j.paerosci.2014.07.001.
[13] Gremlins program demonstrates airborne recovery, DARPA (2021) https://www.darpa.mil/newsevents/2021-11-05. (accessed 10 August 2022).
[14] S. Stappert, J. Wilken, L. Bussler, M. Sippel, A Systematic assessment and comparison of reusable first stage return options, IAC-19-D2.3.10, 70th International Astronautical Congress, Washington D.C., USA, 2019 21-25 October.
[15] E.J. Saltzman, Aerodynamic Assessment of Flight-Determined Subsonic Lift and Drag Characteristics of Seven Lifting-Body and Wing-body Reentry Vehicle Configurations, National Aeronautics and Space Administration, Dryden Flight Research Center, 2002.
[16] R. Martinez-Val, E. Perez, J.F. Palacin, Historical evolution of air transport productivity and efficiency, AIAA 2005-121, 43rd AIAA Aerospace Sciences Meeting and Exhibit, 2005 10-13 January.
[17] M. Sippel, S. Stappert, L. Bussler, C. Messe, Powerful and Flexible Future Launchers in 2-or 3-stage Configuration, IAC-19-D2.4.8, 70th International Astronautical Congress, 2019 21-25 October.
[18] A340-600 global performer, Previous Generation Aircraft (2022) https://www.airbus.com/aircraft/previous-generationaircraft/a340family/a340600.html. (accessed 21 August 2022).
[19] M. Sippel, S. Stappert, L. Bussler, S. Callsen, High-performance, partially reusable launchers for Europe, IAC-20-D2.4.1, 71st International Astronautical Congress (IAC), 2020 12-14 October.
[20] M. Sippel, S. Stappert, S. Callsen, I. Dietlein, K. Bergmann, A. Gülhan, P. Marquardt, A viable and sustainable European path into space – for cargo and astronauts, IAC-21-D2.4.4, 72nd International Astronautical Congress (IAC), UAE, Dubai, 2021 25-29 October.
[21] S. Singh, L. Bussler, S. Stappert, M. Sippel, C.Y. Kucukosman, S. Buckingham, Simulation and analysis of pull-up manoeuvre during in-air capturing of a reusable launch vehicle, 9th European Conference for Aeronautics and Space Sciences (EUCASS), Lille, France, 2022 27 June –1 July.
[22] G.J.D. Calabuig, Conceptual cost estimation for recovery and refurbishment operations of reusable launch vehicles, SART TN-006/2019, DLR (2019) https://elib.dlr.de/144125/. (accessed 10 August 2022).
[23] S. Stappert, J. Wilken, G.J.D. Calabuig, M. Sippel, Cost estimation in the preliminary design phase of reusable launch vehicles, 9th European Conference for Aeronautics and Space Sciences (EUCASS), Lille, France, 2022 27 June –1 July.
[24] AirbusAircraft Characteristics Airport and Maintenance Planning, A340-500/-600, Airbus SAS France, 2005.
[25] J. Williams, S. Vukelich, USAF Stability and Control DATCOM, Volume 2: Implementation of DATCOM Methods, Air Force Flight Dynamics Laboratory, 1976.
[26] J.D. Anderson, Fundamentals of Aerodynamics, McGraw, 2009.
[27] S. Singh, S. Stappert, S. Buckingham, S. Lopes, Y.C. Kucukosman, M. Simioana, M. Pripasu, A. Wiegand, M. Sippel, P. Planquart, Dynamic Modelling and control of an aerodynamically controlled capturing device for 'in-air-capturing' of a reusable launch vehicle, in: 11th International ESA Conference on Guidance, Navigation & Control Systems, 2021, pp. 22–25.
[28] A.C. Kermode, Mechanics of flight, longman scientific and technical, 1987.
[29] P.H. Zipfel, Modelling and Simulation of Aerospace Vehicle Dynamics, 2nd Edition, AIAA, 2007.
[30] Simscale documentation: k-Omega and k-Omega SST, 2022 https://www.simscale.com/docs/simulationsetup/global-settings/k-omega-sst/, (accessed 31 August 2022)
[31] European Aviation Safety Agency, EASA type certificate data sheet, type: rolls-Royce plc RB211 Trent 500 Series engine, 2007, 26 October.
[32] Federal Aviation AdministrationAirplane Flying Handbook, FAA-H-8083-3B, 2016.
[33] P.P. Walsh, P. Fletcher, Gas Turbine Performance, John Wiley & Sons, 2004.
[34] J.F. Marchman, Introductory Flight Performance, 2nd Edition, 2001.
[35] S. Singh, M. Simioana, S. Stappert, M. Sippel, S. Buckingham, S. Lopes, Y.C. Kucukosman, Control design and analysis of a capturing device performing in-air capturing of a reusable launch vehicle, 9th European Conference for Aeronautics and Space Sciences (EUCASS), Lille, France, 2022 27 June –1 July.
[36] S. Singh, S. Stappert, L. Bussler, M. Sippel, Y.C. Kucukosman, S. Buckingham, A full-scale simulation and analysis of formation flight during in-air capturing, 72nd International Astronautical Congress (IAC), Dubai, UAE, 2021 25-29 October.
[37] L.E. Briese, B. Gäßler, Advanced modeling and trajectory optimization of the in-air-capturing maneuver for winged RLVs, Acta Astronaut. 193 (2021) 756766, doi:10.1016/j.actaastro.2021.09.005.